ISSN 1674-1056
http://cpb.iphy.ac.cn
http://iopscience.iop.org/cpb
中国物理 B
Chinese Physics
中国物理
Chinese Physics B

Investigation on flow field characteristics during the impact of a gaseous jet on liquid-water column

Jian Wang(王健), Wen-Jun Ruan(阮文俊), Hao Wang(王浩), Li-Li Zhang(张莉莉)

Citation: Chin. Phys. B . 2019, 28(6): 064704. **doi:** 10.1088/1674-1056/28/6/064704
Journal homepage: http://cpb.iphy.ac.cn; http://iopscience.iop.org/cpb

What follows is a list of articles you may be interested in

Investigation of convergent Richtmyer-Meshkov instability at tin/xenon interface with pulsed magnetic driven imploding

Shaolong Zhang(张绍龙), Wei Liu(刘伟), Guilin Wang(王贵林), Zhengwei Zhang(章征伟), Qizhi Sun(孙奇志), Zhaohui Zhang(张朝辉), Jun Li(李军), Yuan Chi(池原), Nanchuan Zhang(张南川)

Chin. Phys. B . 2019, 28(4): 044702. **doi:** 10.1088/1674-1056/28/4/044702

Three-dimensional multi-relaxation-time lattice Boltzmann front-tracking method for two-phase flow

Hai-Qiong Xie(谢海琼), Zhong Zeng(曾忠), Liang-Qi Zhang(张良奇)

Chin. Phys. B . 2016, 25(1): 014702. **doi:** 10.1088/1674-1056/25/1/014702

Laser-driven flier impact experiments at the SG-III prototype laser facility

Shui Min, Chu Gen-Bai, Xin Jian-Ting, Wu Yu-Chi, Zhu Bin, He Wei-Hua, Xi Tao, Gu Yu-Qiu

Chin. Phys. B . 2015, 24(9): 094701. **doi:** 10.1088/1674-1056/24/9/094701

Lattice Boltzmann simulation of liquid–vapor system by incorporating a surface tension term

Song Bao-Wei, Ren Feng, Hu Hai-Bao, Huang Qiao-Gao

Chin. Phys. B . 2015, 24(1): 014703. **doi:** 10.1088/1674-1056/24/1/014703

Multi-relaxation-time lattice Boltzmann front tracking method for two-phase flow with surface tension

Xie Hai-Qiong, Zeng Zhong, Zhang Liang-Qi, Liang Gong-You, Hiroshi Mizuseki, Yoshiyuki Kawazoe

Chin. Phys. B . 2012, 21(12): 124703. **doi:** 10.1088/1674-1056/21/12/124703

Studies of flow field characteristics during the impact of a gaseous jet on liquid–water column*

Jian Wang(王健)[1,†], Wen-Jun Ruan(阮文俊)[1], Hao Wang(王浩)[1], and Li-Li Zhang(张莉莉)[2]

[1] *School of Energy and Power Engineering, Nanjing University of Science and Technology, Nanjing* 210094, *China*
[2] *Harbin Jian Cheng Bloc Limited Company, Harbin* 150030, *China*

(Received 8 January 2019; revised manuscript received 15 March 2019; published online 29 May 2019)

Both experimental and numerical studies were presented on the flow field characteristics in the process of gaseous jet impinging on liquid–water column. The effects of the impinging process on the working performance of rocket engine were also analyzed. The experimental results showed that the liquid–water had better flame and smoke dissipation effect in the process of gaseous jet impinging on liquid–water column. However, the interaction between the gaseous jet and the liquid–water column resulted in two pressure oscillations with large amplitude appearing in the combustion chamber of the rocket engine with instantaneous pressure increased by 17.73% and 17.93%, respectively. To analyze the phenomena, a new computational method was proposed by coupling the governing equations of the MIXTURE model with the phase change equations of water and the combustion equation of propellant. Numerical simulations were carried out on the generation of gas, the accelerate gas flow, and the mutual interaction between gaseous jet and liquid–water column. Numerical simulations showed that a cavity would be formed in the liquid–water column when gaseous jet impinged on the liquid–water column. The development speed of the cavity increased obviously after each pressure oscillation. In the initial stage of impingement, the gaseous jet was blocked due to the inertia effect of high-density water, and a large amount of gas gathered in the area between the nozzle throat and the gas–liquid interface. The shock wave was formed in the nozzle expansion section. Under the dual action of the reverse pressure wave and the continuously ejected high-temperature gas upstream, the shock wave moved repeatedly in the nozzle expansion section, which led to the flow of gas in the combustion chamber being blocked, released, re-blocked, and re-released. This was also the main reason for the pressure oscillations in the combustion chamber.

Keywords: gaseous jet, liquid–water column, pressure oscillations, shock wave

PACS: 47.61.Jd, 47.60.Kz, 47.40.Nm, 47.27.wg **DOI:** 10.1088/1674-1056/28/6/064704

1. Introduction

The solid rocket engine will form a high temperature gaseous jet when it works and there are periodic shock waves in both axial and radial directions of the jet flow field.[1] These shock waves interact with turbulent structures along the jet shear layer, producing screech and broadband shock-associate noise in addition to the classical mixing noise.[2] These characteristics will cause harm to the surrounding environment and staff. For a long time, reducing the temperature and noises of the gaseous jet has become an important subject in experimental, theoretical, and numerical investigations. Geery[3] first used water injection to reduce the temperature and noises of gaseous jet. In the process of injecting water into the gaseous jet, strong energy exchange and momentum exchange occur between the liquid–water and the gaseous jet, reducing the temperature and speed of the gaseous jet, thus achieving the goals of cooling and noises reduction. However, factors such as water injection mode and water mass flow rate will have a significant impact on the cooling and noises reduction effects.[4–11] In the design of AT4 C-S shoulder-fired rocket, Sweden put forward the way of placing liquid–water column in the tail pipe of the launcher to weaken the launch characteristics. Zhang *et al.*[12] had carried out an experimental study on noises reduction effect of this method and this experimental result showed that after the liquid–water column was placed in the tail pipe, the peak value of sound pressure at each measuring point arranged in the flow field was obviously reduced. Although the liquid–water column had a good cooling and noises reduction effect on the gaseous jet of the shoulder-fired rocket, when the solid rocket engine worked, the high temperature and high pressure gas generated in the combustion chamber would impinge the liquid–water column after passing through the nozzle. Heat and mass transfer, phase transition, and other phenomena would occur between the gas phase and liquid phase, accompanied by complex wave system transfer and hydrodynamic interference. This impinging process was equivalent to a slight underwater explosion and would have an influence on the performance of the rocket engine. At present, there are no complete and mature studies to give a reasonable explanation and accurate prediction of the influence of impinging process on the rocket engine performance. The existing gas–liquid multiphase flow numerical calculation methods also cannot completely describe the gas generation process, the gas acceleration process in the nozzle, and the coupled flow

*Project supported by the National Natural Science Foundation of China (Grant No. 51305204).
†Corresponding author. E-mail: 1805322964@qq.com
© 2019 Chinese Physical Society and IOP Publishing Ltd

process with liquid–water column.[13–24] Therefore, this paper designed an experimental platform for the study of gaseous jet impinging on liquid–water column, and investigated the influence of impinging process on the rocket engine performance experimentally. After that, a new computational method was proposed by coupling the governing equations of MIXTURE model with the phase change equations of water and the combustion equation of propellant. Numerical simulation on the whole process of gaseous jet impinging on liquid–water column was carried out and the flow field characteristics were analyzed.

2. Experimental research

2.1. Experimental device and schematic design

In order to eliminate the influence of gravity on the jet flow field, a vertically placed experimental device was designed. The gas was jetted vertically upwards and the structure of the experimental device is shown in Fig. 1, mainly combined by the base, the combustion chamber, the connecting pipe, the nozzle, the tail pipe, the liquid–water column, etc. For ease of installation, the liquid–water was enclosed in a thin-walled cylindrical plastic tube and placed in the tail pipe. The working principle of the experimental device was using the electric ignition device to ignite the propellant filled in the combustion chamber. High temperature and high pressure gas was generated when the propellant burned rapidly. When the pressure in the combustion chamber increased to a certain level, the diaphragm at the throat of the nozzle was flushed to broken, and the gas was accelerated by the nozzle to form a supersonic gaseous jet. If the liquid–water column was placed in the tail pipe, the gaseous jet would impinge the liquid–water column and sprayed into the atmosphere in the process of interacting with water. The experiment was carried out under two conditions: (i) the investigation of gaseous jet flow field without liquid–water column; (ii) the investigation of gas–liquid mixed flow field formed by gaseous jet impinged the liquid–water column.

In order to obtain the working characteristics of the rocket engine and flow field characteristics under two experimental conditions, the relevant measurement system was designed in this experiment. At point 1 and point 2 shown in Fig. 1, a KISTLER-601 H piezoelectric pressure sensor manufactured by KISTLER Company was placed respectively. The DEWE-4010 transient data recorder made by the company of LABG was used to record the change process of pressure in the combustion chamber and tail pipe. Due to the complexity of the unsteady gaseous jet flow field and the gas–liquid mixed flow field, each point in the flow field had a strong random fluidity, and it was difficult to mark and track the flow at a certain point. Therefore, this experiment used the image acquisition system to record the flow field formed under each experimental condition, and qualitatively obtained the change of the flow field structure. The system consisted of a high-speed camera and an image processing computer. In order to reduce the error caused by the external environment to the experimental results, this experiment was carried out in an open field, the ambient temperature was about 25 ℃, the air humidity was less than 50%, and the wind speed was less than level 3. The experimental device was installed on a concrete column platform at a certain height from the ground.

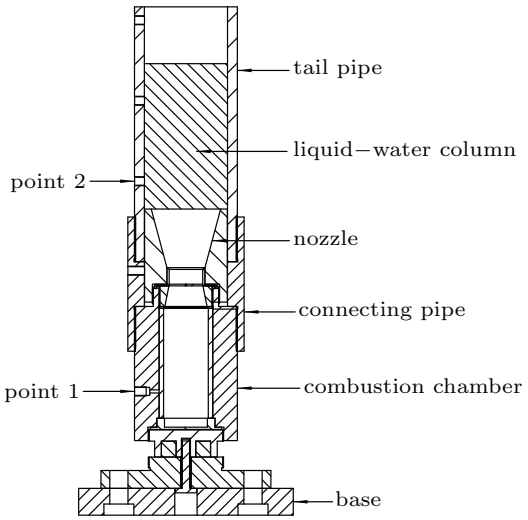


Fig. 1. The schematic diagram of experimental apparatus.

2.2. Experimental results and analysis

Figure 2 shows the expansion process of gaseous jet and gas–liquid mixed jet in the atmospheric environment captured by high-speed camera. It can be seen from the figure that in the case of a liquid-free water column, the gaseous jet expanded in the axial direction significantly faster than the radial expansion speed. Due to the higher temperature of the gas, the interior of the jet flow field exhibited high brightness characteristics. After $t = 35$ ms, A large amount of white smoke began to appear at the exit of the tail pipe and at the edge of the jet flow field, which was formed by the condensed particles in the propellant combustion products.

Under the experimental condition that the liquid–water column was placed in the tail pipe, the gas would first impinge the liquid–water column when the gas flowed out from the nozzle. After that, the gas and the liquid–water jointly ejected from the tail pipe in the process of strong mixing and formed the gas–liquid mixed jet flow field. Due to the hindrance of the water column, the time of gas–liquid mixed jet ejecting from the tail pipe was lagged behind that of gaseous jet. The axial direction of the jet flow development speed also became slow. As shown in Fig. 2(b), at $t = 36$ ms, the outer contour of the gas–liquid mixed jet flow field gradually began to appear jagged, showing strong instability at the gas–liquid

interface. This instability would cause the liquid to break up, and a large number of small droplets appeared and increased the vaporization surface of the liquid, which helped the liquid–water vaporize to absorb more gas energy, further reducing the temperature of the flow field. The high brightness characteristics were no longer visible compared with the gaseous jet flow field without the liquid column. At the same time, due to the atomization of the liquid–water, the entire flow field area was covered by a large amount of water mist, so that the scattering and absorption of light by the particles was not enough to be detected. The white smoke that appeared in the experiment state without liquid–water column no longer appeared.

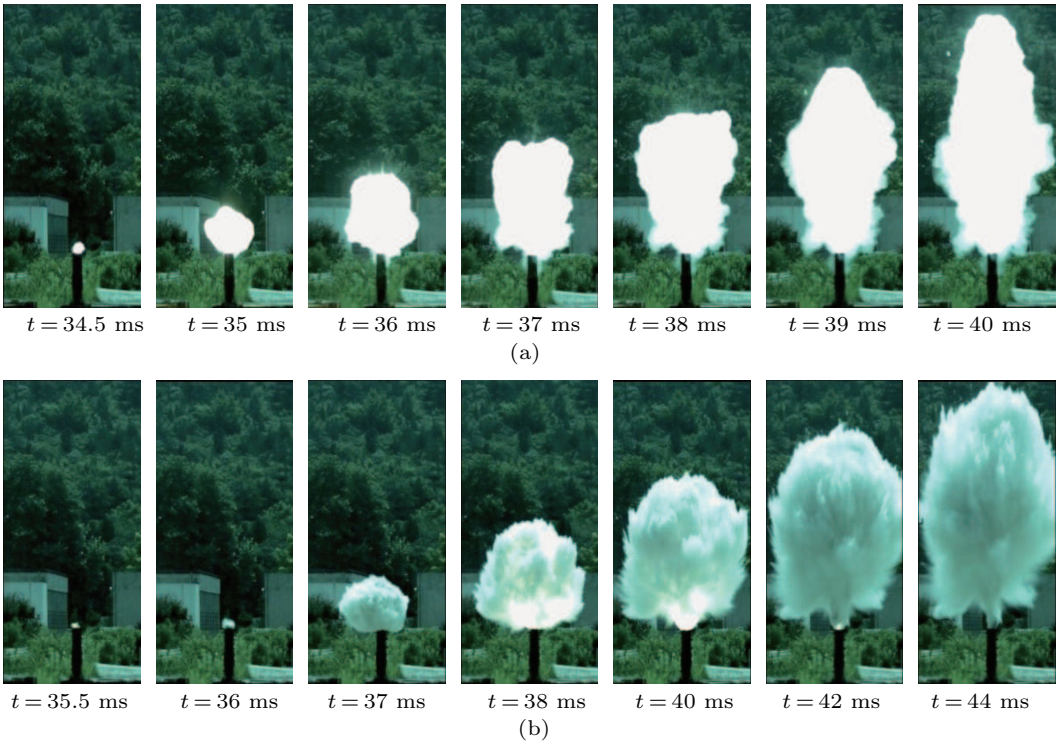


Fig. 2. The distribution of jet flow field in the atmospheric environment at different times. (a) The expansion process of gaseous jet in the atmospheric environment. (b) The expansion process of gas–liquid mixed jet in the atmospheric environment.

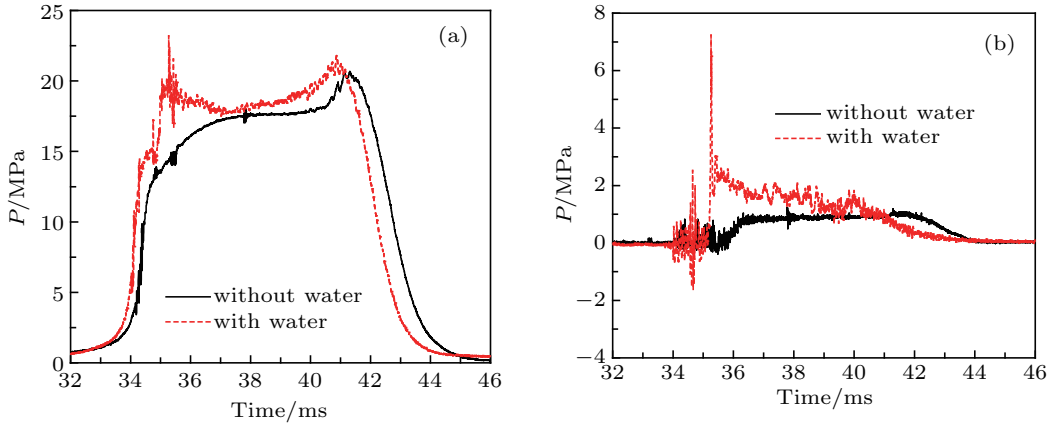


Fig. 3. Pressure change curves in combustion chamber and tail pipe measured by experiment. (a) Pressure change curves in combustion chamber. (b) Pressure change curves in tail pipe.

Figure 3 shows the comparison curves of pressure changed in the combustion chamber and tail pipe under the experimental conditions with or without liquid–water column. Under the experimental condition containing liquid–water column, the pressure in the combustion chamber increased overall, but two pressure oscillations with large amplitude occurred when $t = 34.75$ ms and $t = 35.27$ ms. The instantaneous pressure increased by 17.73% and 17.93% respectively and dropped rapidly after reaching the peak. At the same time point, the pressure in the tail pipe also had two pressure oscillations with large amplitude, but after the second oscillation, the pressure in the tail pipe decreased gradually. Under the experimental condition without liquid–water column, the changes of pressure in the combustion chamber and tail pipe were relatively stable, and there were relatively gentle ascending, working, and descending stages. However, the pressure

rising stage in the combustion chamber between $t = 41$ ms and $t = 42$ ms may be caused by the uneven combustion of propellant at the end of rocket working.

3. Numerical calculation

It can be seen from the above experimental results that although the liquid–water column has a better flame and smoke dissipation effect for the gaseous jet, however, the interaction process between gaseous jet and liquid–water column is very complicated and it has a great influence on the working performance of rocket. Therefore, it is necessary to have a clearer understanding of gas–liquid mixed flow field structure formed by gas jet impinging on liquid–water column. In this article, the phase change equations of water, the combustion equation of propellant, and the governing equations of MIXTURE model are coupled to simulate the process of gaseous jet impinging on the liquid–water column. The gas–liquid mixed flow field structure and the reason of pressure oscillations are further analyzed and researched.

3.1. Formulation of numerical models

The process of gaseous jet impinging on the liquid–water column involves complex multiphase flow problems. In order to achieve effective calculation, this article adopts a simplified physical model and proposes the following assumptions: (I) the actual three-dimensional flow problem is simplified into a two-dimensional turbulent flow, which is considered as an unsteady expansion process; (II) the combustion product of propellant is assumed as an ideal gas with a single component, and a frozen isentropic flow model is adopted, that is, the composition of the combustion product of gas phase does not change with the change of temperature and pressure; (III) only the gas phase is the compressible phase, and the liquid phase and the water–vapor phase are both incompressible phases; (IV) the heat exchange between the gas and the walls is not considered because of the gas in the experimental device flowed at a high speed. In other words, the walls are regarded as adiabatic and non-slip walls.

According to the assumptions of the above physical models, the following numerical equations are established.

The continuity equation is defined as

$$\frac{\partial}{\partial t}(\rho_{\mathrm{m}}) + \nabla \cdot (\rho_{\mathrm{m}} \boldsymbol{u}_{\mathrm{m}}) = m_{\mathrm{S}}. \tag{1}$$

In Eq. (1), t is the time, ρ_{m} is the density of the mixture, ∇ is the Hamiltonian operator, $\boldsymbol{u}_{\mathrm{m}}$ is the average velocity of the mixture, and m_{S} is the custom quality source item. According to the combustion equation of propellant used in the experiment, m_{S} is expressed as

$$m_{\mathrm{S}} = \rho_{\mathrm{G}} \cdot \left[a \left(p_{\mathrm{v}} / 10^6 \right)^b \right] \cdot 10^{-3} \cdot S. \tag{2}$$

where ρ_{G} is the density of propellant, a is the burning rate coefficient of propellant, p_{v} is the average pressure in the combustion chamber, b is the burning rate index, and S is the burning surface area of propellant.

The momentum conservation equation can be obtained by summing the momentum equations of each phase, which can be expressed as

$$\begin{aligned} &\frac{\partial}{\partial t}(\rho_{\mathrm{m}} \boldsymbol{u}_{\mathrm{m}}) + \nabla \cdot (\rho_{\mathrm{m}} \boldsymbol{u}_{\mathrm{m}} \boldsymbol{u}_{\mathrm{m}}) \\ &= -\nabla p + \nabla \cdot \left[\mu_{\mathrm{m}} \left(\nabla \boldsymbol{u}_{\mathrm{m}} + \nabla \boldsymbol{u}_{\mathrm{m}}^{\mathrm{T}} \right) \right] + \rho_{\mathrm{m}} \boldsymbol{g} \\ &\quad + \boldsymbol{F} + \nabla \cdot \left(\sum_{k=1}^{n} \alpha_k \rho_k \boldsymbol{u}_{\mathrm{d}r,k} \boldsymbol{u}_{\mathrm{d}r,k} \right). \end{aligned} \tag{3}$$

In Eq. (3), p is the local pressure at each node, μ_{m} is the mixed viscosity, $\boldsymbol{g}$ is the gravity acceleration, $\boldsymbol{F}$ is the volume force, k stands for the k phase, and n stands for the total number of phases. There are three phases in the numerical models of this article, namely, the gas phase at $k = 1$, the liquid phase at $k = 2$, and the water–vapor phase at $k = 3$.α_k represents the volume fraction of the k phase, ρ_k is the density of the k phase, and $\boldsymbol{u}_{\mathrm{dr,k}}$ is the drift speed of the k phase.

The energy conservation equation is defined as

$$\begin{aligned} &\frac{\partial}{\partial t} \sum_{k=1}^{n} (\alpha_k \rho_k E_k) + \nabla \cdot \sum_{k=1}^{n} \left[\alpha_k \boldsymbol{u}_k (\rho_k E_k + p) \right] \\ &= \nabla \cdot (k_{\mathrm{eff}} \nabla T_{\mathrm{mix}}) + S_{\mathrm{E}}. \end{aligned} \tag{4}$$

For compressible phase, $E_k = h_k – p/\rho_k + u_k^2/2$. For incompressible phase, $E_k = h_k$, where h_k is the sensible enthalpy of the k phase. k_{eff} is the effective heat conductivity defined according to the turbulence model. T_{mix} is the thermodynamic temperature of the mixture. The first term on the right side of Eq. (4) represents the energy transfer due to heat conduction, and S_{E} represents the energy change caused by gas mass addition and physical phase change of water.

Since only the gas phase is a compressible phase, the state equation of each phase is as follows:

$$\rho_k = \begin{cases} p/RT_1, & k = 1, \\ \text{const}, & k = 2, \\ \text{const}, & k = 3, \end{cases} \tag{5}$$

In Eq. (5), R stands for molar gas constant and T_1 stands for instantaneous temperature of the gas phase.

In order to simulate the vaporization process of water and the condensation process of water–vapor, the physical phase change equations of water are used to calculate it. The state of water at each compute node is determined by the pressure and temperature at that node. When the temperature is higher than the saturation temperature of the liquid–water at the local pressure, the liquid–water absorbs energy and is vaporized into water–vapor. When the temperature is lower than the saturation temperature of the liquid–water at the local pressure, the

water–vapor releases energy and condenses into liquid–water. The physical phase change equations of water are as follows.

The liquid–water–vaporization equation is defined as

$$m_2 = \begin{cases} \beta\alpha_2\rho_2 |T_2 - T_{\text{sat}}| / T_{\text{sat}}, & T_2 \geqslant T_{\text{sat}}, \\ 0, & T_2 < T_{\text{sat}}. \end{cases} \tag{6}$$

The water–vapor condensation equation is defined as

$$m_3 = \begin{cases} 0, & T_3 \geqslant T_{\text{sat}}, \\ \beta\alpha_3\rho_3 |T_3 - T_{\text{sat}}| / T_{\text{sat}}, & T_3 < T_{\text{sat}}. \end{cases} \tag{7}$$

In Eqs. (6) and (7), m_2 and m_3 stand for the vaporization rate of liquid–water and the condensation rate of water–vapor, respectively, T_{sat} is the saturation temperature of liquid–water at the local pressure, T_2 and T_3 are the instantaneous temperatures of the liquid phase and the vapor phase, respectively, and β is the vaporization coefficient. According to the above formulas, the instantaneous net vaporization rate of liquid–water can be calculated as

$$m_{\text{V}} = m_2 - m_3. \tag{8}$$

The energy change caused by the phase change is

$$S_{\text{V}} = -\Delta H m_{\text{V}}. \tag{9}$$

In Eq. (9), S_{V} is the energy change caused by phase change, and ΔH is the latent heat of vaporization of saturated water. The energy change caused by mass addition is expressed as

$$S_{\text{m}} = m_{\text{S}} \cdot C_{\text{p}} \cdot T_{\text{p}}, \tag{10}$$

$$S_{\text{E}} = S_{\text{V}} + S_{\text{m}}. \tag{11}$$

In Eqs. (10) and (11), S_{m} is the change in energy due to mass addition, C_{p} is the specific heat of constant pressure, and T_{p} is the burning temperature of constant pressure. In numerical calculation, the energy change S_{E} is substituted into the energy equation by the mode that adds source terms.

In the calculation of multiphase flow, in addition to the continuity equation of the mixture, the volume fraction of each phase should be calculated by the auxiliary continuity equation of gas phase and water–vapor phase.

The gas phase continuity equation is defined as

$$\frac{\partial}{\partial t}(\alpha_1\rho_1) + \nabla\cdot(\alpha_1\rho_1\boldsymbol{u}_{\text{m}}) + \nabla\cdot\left(\alpha_1\rho_1\boldsymbol{u}_{\text{d}r,1}\right) = m_{\text{S}}. \tag{12}$$

The water–vapor phase continuity equation is defined as

$$\frac{\partial}{\partial t}(\alpha_3\rho_3) + \nabla\cdot(\alpha_3\rho_3\boldsymbol{u}_{\text{m}}) + \nabla\cdot\left(\alpha_3\rho_3\boldsymbol{u}_{\text{d}r,3}\right) = m_{\text{V}}. \tag{13}$$

Due to the sum of the volume fraction of all the phases is 1, the volume fraction α_1 and α_3 of the gas phase and the water–vapor phase can be obtained by solving the above continuity equations, thereby obtaining the volume fraction of the liquid phase as $\alpha_2 = 1 - \alpha_1 - \alpha_3$.

3.2. Computational domain and numerical method

Since the formed flow field was a three-dimensional axisymmetric structure, this article has simplified the three-dimensional flow field into a two-dimensional computational domain, including the combustion chamber, nozzle, tail pipe, and external standard atmospheric space, as shown in Fig. 4. The geometries of the combustion chamber, nozzle, and tailpipe were consistent with the dimensions in the experimental structure. The size of the external atmospheric space was $55d \times 40d$ (length $\times$ width), where d was the diameter of nozzle throat. In order to observe the change rule of physical quantity in combustion chamber, one monitoring point was set on the wall of combustion chamber. The location of the monitoring point is the same as that of test point 1 in experimental study. When using non-reflective boundary conditions, this computational domain can ensure that the real flow field parameters can be obtained without the computational boundary interference.

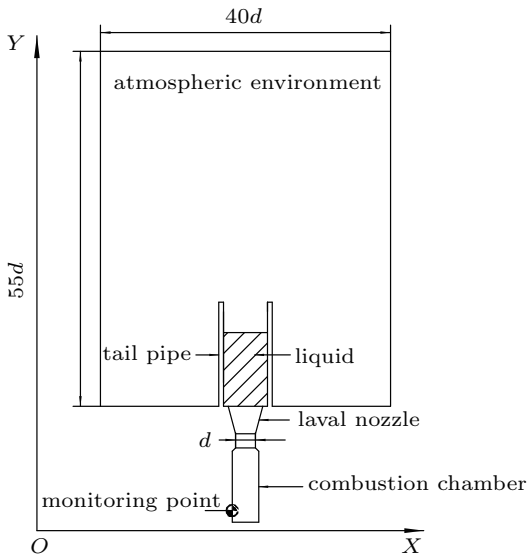


Fig. 4. The computational domain.

In the experiment of gaseous jet impinging on the liquid–water column, a pressure limiting diaphragm was placed at the throat of the nozzle. When the pressure in the combustion chamber reached the membrane breaking pressure, the gas flowed out from the nozzle and impinged the liquid–water column. Therefore, in this article, the whole calculation area was divided into two parts, and the combustion chamber and the nozzle contraction section were divided into region 1. The region 1 was set as a region continuously producing gas by using the method of defining source items to simulate the combustion process of the propellant in the combustion chamber. The nozzle expansion section, the tail pipe, and the external atmospheric environment were divided into region 2. At the time of initialization, the corresponding area in the tail pipe was designated as the water area according to the size of the liquid–water column in the experiment, and the other regions were the

standard static atmospheric environment. The boundaries of the combustion chamber, the nozzle, and the tail pipe were set to the wall boundary condition, and the boundaries of the external atmospheric environment were set as the pressure outlet boundary condition. In this article, the finite volume method was used to discretize the governing equation. The turbulence model used a model with swirl correction (realizable model) to describe the process of interaction between gaseous jet and liquid–water. The wall surfaces were selected without slip and adiabatic wall conditions, and the near wall adopted the standard wall function method to treat turbulence. The pressure-implicit with splitting of operators (PISO) algorithm was used to solve the coupling of pressure and velocity, volume fraction equations were discrete by using the QUICK format, and the pressure term was discrete by using the PRESTO method. The other diffusion terms, convection terms, and the discrete formats of turbulent k and ε equation all adopted the first-order upwind style.

3.3. Numerical results and analysis

Based on the computational domain established in the previous section and the numerical calculation method, the unsteady process of gaseous jet impinging on the liquid–water column was numerically calculated in this paper. Due to the high sampling frequency and large amount of data stored in the data acquisition system, this paper selected the pressure data of one hundred time points in the experimental results for comparative analysis with the numerical calculation results. Figure 5 shows the comparison between the experimental and the numerical pressure results at the monitoring point. It can be seen from Fig. 5 that the numerical calculation results are consistent with the change trend of the experimental results relative to time, which can reflect the pressure change law at the monitoring point in the process of gaseous jet impinging on the liquid–water column, indicating that the mathematical model and calculation method established in this paper were reasonable and feasible. As can be seen from Fig. 5, when the pressure in the combustion chamber reached the stable working period, the pressure values obtained by numerical calculation were slightly higher than that measured in the experiment.

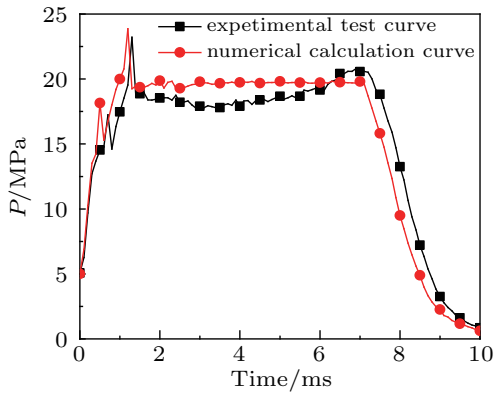


Fig. 5. The comparison diagram of experimental results and numerical results.

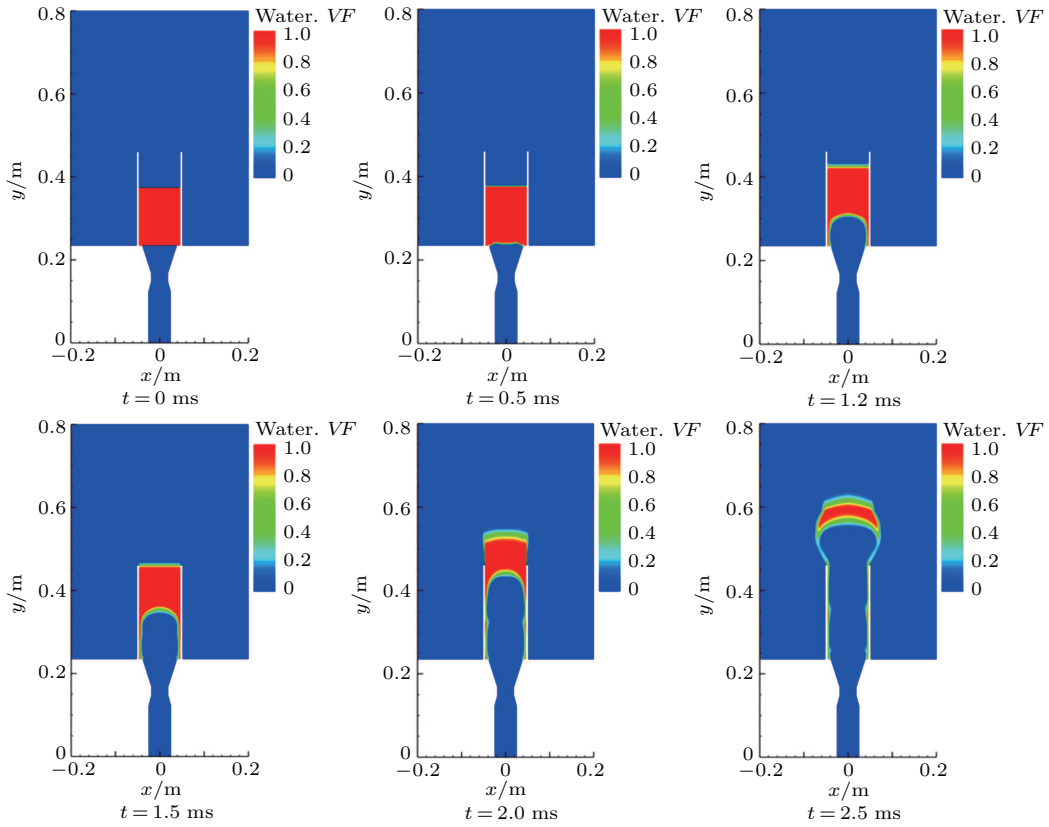


Fig. 6. The distribution diagram of water volume fraction at different times.

This may be due to the incomplete burning of propellant in the combustion chamber during the experiment study and the mixed jet inevitably caused some energy losses in the actual flow process. There are twice obvious pressure oscillations with large amplitude in both experimental and numerical results. The causes for pressure oscillations at the monitoring point would be analyzed according to the following numerical results.

Since the liquid–water column had little influence on the working performance of rocket after being completely pushed out of the tail pipe by gaseous jet, this paper only selected the calculation results within 2.5 ms from the beginning of the impingement for analysis and research. Figure 6 shows the distribution of water volume fraction in the gas–liquid mixed jet flow field at different times.

Figure 7 shows the time-dependent curve of the development distance of the cavity along the axis in the liquid–water column. Combining Figs. 6 and 7, it can be seen that when $t = 0.2$ ms, the gaseous jet began to impinge the liquid–water column. The gas–liquid interface produced obvious displacement, and the gas gradually formed a cavity in the liquid–water column. Due to the small amount of gas generated

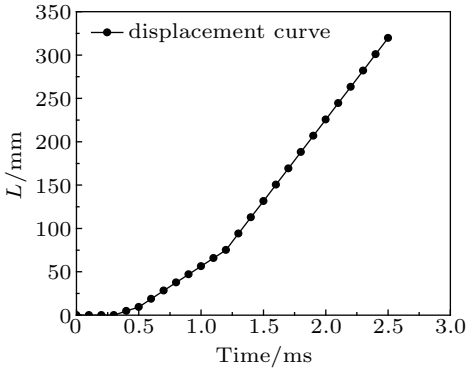


Fig. 7. The cavity displacement curve.

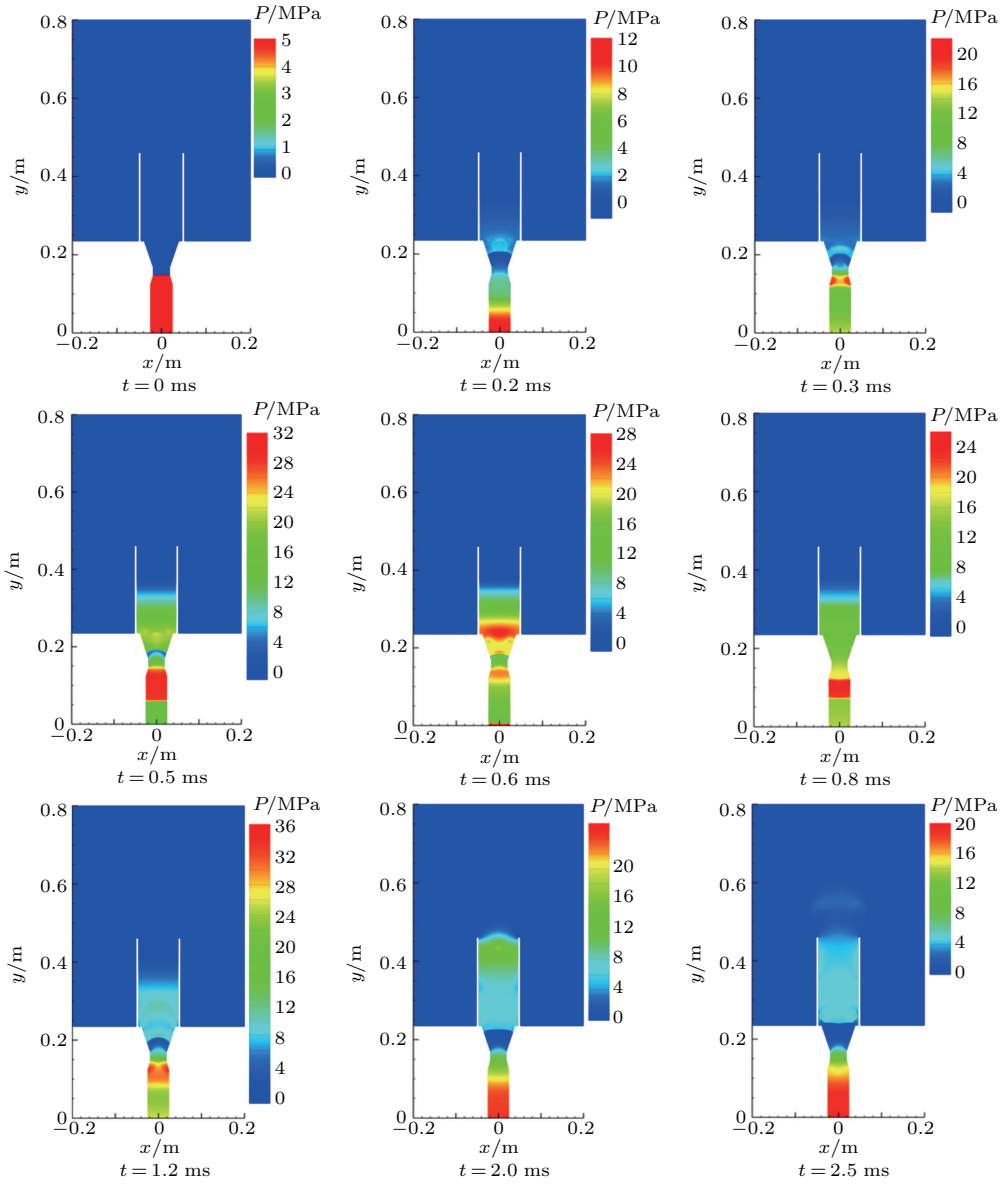


Fig. 8. The cloud diagrams of pressure distribution at different times.

at this time, the pressure in front of gas–liquid interface was low, resulting in a slow increase in the speed of the cavity. However, with the development of the flow field, the development speed of the cavity increased significantly at $t = 0.5$ ms and $t = 1.2$ ms, which was consistent with the time when the two pressure oscillations in the combustion chamber reached their peak values. When $t = 1.2$ ms, the head of the cavity presented a regular semicircle. After that, the water moved forward along both sides of the pipe wall under the push of the gaseous jet, and the shape of the gas–liquid interface did not change significantly during the movement. When $t = 2.5$ ms, only a little residual water in the tail pipe adhered to the pipe wall, and the flow field started to develop along the radial direction without the constraint of the pipe wall. Because the gaseous jet pushed the liquid–water column to move in the tail pipe for only 2.5 ms, the action time was relatively short, so the liquid was not vaporized completely and most of the water was still sprayed into the external atmosphere environment.

The cloud diagrams of pressure distribution in the computational domain at different times were shown in Fig. 8. The moment when the gaseous jet broke through the diaphragm at the nozzle throat was taken as the initial time of numerical calculation. At this time, the membrane breaking pressure of 5 MPa was evenly distributed in the combustion chamber.

As can be seen from the figure, when the diaphragm was broken, the gaseous jet flowed rapidly into the expansion section of the nozzle, resulting in a pressure decrease near the nozzle inlet in the combustion chamber. At this time, the gas near the bottom of the combustion chamber flowed relatively slow, and the pressure near the bottom of the combustion chamber rose rapidly with the rapid combustion of the propellant. Due to the inertia effect of the high-density water, the gaseous jet was blocked by liquid–water column, and a large amount of gas accumulated in the nozzle expansion section, which leads to the pressure rise in this region and the shock wave formation in the nozzle expansion section. With the combustion of propellant and the flow of gas, the pressure after shock wave increased continuously, and the phenomenon of pressure wave back propagation was formed. Under the action of reverse pressure wave, the shock wave moved along the nozzle expansion section towards the nozzle throat. Therefore, within the time frame from $t = 0.3$ ms to $t = 0.5$ ms, the pressure near the nozzle inlet in the combustion chamber increased sharply and continuously extended to the combustion chamber interior. When $t = 0.5$ ms, the pressure reached the maximum value, which also corresponded to the wave peak of the pressure oscillation of the first time at monitoring point 1. When the pressure at the nozzle inlet and the pressure at the nozzle outlet reached a certain ratio, the gas could flow smoothly from the combustion chamber into the nozzle again, so the pressure in the combustion chamber decreased quickly. However, since the liquid–water only produced very small motion at this time, the gas once again accumulated in large quantity between the nozzle throat and the gas–liquid interface. The reverse pressure wave caused the shock wave to move in the opposite direction again and the flow of gas was blocked again, resulting in the emergence of the second time pressure oscillation at $t = 1.2$ ms. At this time, the peak value of the second time pressure oscillation also increased because the gas production of propellant combustion was significantly increased compared with the first time pressure oscillation. Thereafter, the liquid–water column moved rapidly to the external atmospheric environment under the push of high-pressure gas. With the continuous increase of the free volume in the tail pipe, the pressure in the combustion chamber gradually reached a relatively stable working state. During this period, the shock wave in the nozzle expansion section also began to move from the nozzle throat to the nozzle outlet. Until $t = 2.5$ ms, when most liquid–water had been ejected from the tail pipe, the shock wave had moved from the nozzle expansion section to the tail pipe interior. After that, the influence of the interaction between gas and liquid–water on the working performance of the rocket was trivial.

4. Conclusions

In this paper, the process of gaseous jet impinging on the liquid–water column was experimentally studied and a new computational method was proposed to numerically simulate this process. The following conclusions were drawn.

(A) Experimental results showed that the liquid–water had better flame and smoke dissipation effect on gaseous jet. However, the interaction between the gaseous jet and the liquid–water column led to strong pressure oscillations in the combustion chamber of the rocket, which had a great influence on the normal working of the rocket.

(B) To effectively simulate this process, a new numerical method was proposed by coupling the governing equations of MIXTURE multiphase flow calculation model with the phase change equations of water and the combustion equation of propellant. Numerical simulations were successfully carried out and the obtained results were in good agreement with the experimental results.

(C) Through numerical simulation, it was found that a cavity was formed in the liquid–water column when gaseous jet impinged on the liquid–water column. In the initial stage of the impingement, the speed of the cavity was slowly increased. However, after the pressure in the combustion chamber reached the peak of each pressure oscillation, the development speed of cavity increased obviously. Due to the short action time of impingement, the liquid–water was not vaporized completely in the tail pipe and most of the water was still sprayed into the external atmosphere environment.

(D) It was found that in the initial stage of impingement, due to the hindrance of liquid–water, a large amount of gas was gathered in the area between the nozzle throat and the gas–liquid interface. The pressure in this area was increased significantly, and the shock wave was formed in the nozzle expansion section. Under the dual action of the reverse pressure wave and the continuously ejected high-temperature gas upstream, the shock wave moved repeatedly in the nozzle expansion section, which caused the flow of gas in the combustion chamber to be blocked, released, re-blocked, and re-released. This was also the main reason for the pressure oscillations in the combustion chamber.

(E) With the rapid movement of the cavity and the continuous increase of the free volume in the tail pipe, the pressure in the combustion chamber gradually reached a relatively stable state. The shock wave gradually moved to the nozzle outlet, and the phenomenon of repeated movement no longer appeared. At $t = 2.5$ ms, the shock wave had moved into the tail pipe interior when the liquid–water column had been ejected from the tail pipe. After that, the influence of the interaction between gas and liquid–water on the working performance of the rocket was trivial.

References

[1] Vuorinen V, Yu J Z, Tirunagari S, Kaario O, Larmi M, Duwig C and Boersma B J 2013 *Phys. Fluids* **25** 016101

[2] Li X P, Zhou R, Chen X P, Fan X J and Xie G S 2018 *Chin. Phys. B* **27** 094705

[3] Geery E and Greenwood R 1969 *5th Propulsion Joint Specialist* June 9–13, 1969, Colorado Springs, USA, p. 514

[4] Ignatius J K, Sathiyavageeswaran S and Chakravarthy S R 2015 *AIAA J.* **53** 235

[5] Zoppellari E and Juve D 1998 *4th AIAA/CEAS Aeroacoustics Conference*, June 2–4, 1998, Toulouse, France, p. 35

[6] Sankaran S, Ignatius J K, Ramkumar R, Satyanarayana T N V, Chakravarthy S R and Panchapakesan N R 2009 *J. Spacecr. Rockets* **46** 1164

[7] Jiang Y, Ma Y L, Wang W C and Shao L W 2010 *Chin. J. Aeronaut* **23** 653

[8] Li J, Jiang Y, Yu S Z and Zhou F 2015 *Energies* **8** 13194

[9] Kandula M 2008 *AIAA J.* **46** 2714

[10] Fukuda K, Tsutsumi S, Shimizu T and Takaki R 2011 17*th AIAA/CEAS Aeroacoustics Conference*, June 5–8, 2011, Portland, USA, p. 092407

[11] Wang Z G, Wu L Y, Li Q L and Li C 2014 *Appl. Phys. Lett.* **105** 134102

[12] Zhang L, Wang H and Ruan W J 2016 *Acoust. Aust.* **44** 291

[13] Arghode V K and Gupta A K 2012 *Appl. Energy* **89** 246

[14] Shi H H, Wang B Y and Dai Z Q 2010 *Sci. Chin. Phys. Mech.* **53** 527

[15] Zhao H Y and Bhabra B 2018 *Int. J. Multiphase Flow* **105** 74

[16] Tang Y L, Li S P, Liu Z, Sui X and Wang N F 2015 *Acta. Phys. Sin.* **64** 234702 (in Chinese)

[17] Xu H, Wang C, Lu H Z and Huang W H 2018 *Acta. Phys. Sin.* **67** 014703 (in Chinese)

[18] Mohamad T I 2015 *Fuel* **160** 386

[19] Hong S J, Park G C, Cho S and Song C H 2012 *Int. J. Multiphase Flow* **39** 66

[20] Li S P, Tang Y L, Tang J N and Wang N F 2017 55*th AIAA Aerospace Sciences Meeting*, January 9–13, 2017, Grapevine, USA, p. 8

[21] Weil, C and Vlachos P P 2013 *Int. J. Multiphase Flow* **48** 46

[22] Liu G, Wang Y S, Zang G J and Zhao H T 2015 *Int. J. Heat Mass Transfer* **84** 592

[23] Xu H, Fan P F, Ma Y, Guo X S, Yang P, Tu J and Zhang D 2017 *Chin. Phys. B* **26** 024301

[24] Ren G W, Zhang S W, Hong R K, Tang T G and Chen Y T 2016 *Chin. Phys. B* **25** 086202